RSC Advances

PAPER

View Article Online
View Journal | View Issue

Cite this: *RSC Adv.*, 2026, **16**, 17393

Smartphone-integrated sensing platform based on a "one-stone-three-birds" strategy for real-time quantitative detection of Ag(I) ions

Lihua Zhang, * Jiang Li, Tengyan Gao, Wei Liu, Zirui Zhang, Zezhong Chen and Feng Feng *

Heavy metal ion contamination poses a serious threat to human health and ecological balance, emphasizing the need for sensitive detection methods to maintain water quality and safeguard public safety. To meet this challenge, an integrated quantitative detection platform based on smartphone image capture and a built-in RGB color analysis app, following a "one-stone-three-birds" strategy, was developed. It allows for rapid, sensitive, and on-site detection of silver ions (Ag(I)) in actual water samples. In the presence of Ag(I) ions, the aggregation of AuNPs with ammonium thioglycolate (ATG), which acts as a multifunctional agent (an aggregation inducer, charge modulator, and recognition unit), is inhibited, resulting in a notable hypsochromic shift in the surface plasmon resonance (SPR) spectrum of AuNPs and a color change from gray-blue to pink-red, depending on the target level. Quantitative analysis is performed by measuring the color signal intensity of AuNPs after adding Ag(I) ions with a smartphone equipped with an RGB color detector. The detection mechanism was verified further through transmission electron microscopy (TEM), dynamic light scattering (DLS), and UV-Vis spectrophotometry (UV-Vis). The smartphone-integrated detection method exhibited a linear range of 0.1 to 8 μM and a detection limit of 10.4 nM. Results from this platform, paired with a smartphone, were validated against data from atomic absorption spectrometry (AAS). This smartphone-based detection approach offers the benefits of simplicity, speed, and low cost, making it suitable for environmental monitoring of Ag(I) ions.

Received 9th March 2026
Accepted 22nd March 2026

DOI: 10.1039/d6ra02021f

rsc.li/rsc-advances

1 Introduction

With the rapid growth of industry, we must address issues caused by environmental degradation, especially heavy metal pollution. Once heavy metals are released into the environment, even at low levels, they can cause serious health and ecological problems.[1–3] Silver is one of the most toxic heavy metal ions found in land and water ecosystems and is widely used in photography, imaging, batteries, semiconductors, energy, medicine, and other industries.[4] Long-term exposure to high levels of silver ions is known to cause conditions such as silver poisoning, an enlarged heart, skin damage, growth delays, brain damage, and harm to the nervous and immune systems.[5] For example, Ag(I) can bind to metallothionein, macroglobulins, and albumins, potentially disrupting various enzymatic metabolic pathways.[6] Additionally, releasing Ag(I) into aquatic systems can significantly alter the fatty acid composition and other large molecules in microalgae, disrupting their normal functions and posing ecological risks to aquatic environments.[7] Due to these concerns, the World Health Organization (WHO) has set a maximum safe silver level of 0.1 mg L^{-1} (0.93 μM) in drinking water. Therefore, accurately detecting Ag(I) is vital for protecting human health and maintaining ecological balance.

Currently, various effective methods have been developed for detecting and measuring Ag(I) ions, including surface-enhanced Raman scattering,[8–10] surface plasmon resonance (SPR),[11,12] inductively coupled plasma atomic emission spectrometry (ICP-OES),[13] inductively coupled plasma-mass spectrometry (ICP-MS),[14,15] electrochemical techniques,[16–19] atomic absorption spectrometry (AAS),[20] and fluorescence detection.[21–25] However, these methods are costly, time-consuming, labor-intensive, and require complex analyses, making them unsuitable for visual detection by the naked eye and limiting their use in the field. In contrast, emerging smartphone-based colorimetric sensing devices offer portability, simplicity, and the ability to perform visual inspections as a promising tool for the on-site monitoring of Ag(I) ions in environmental samples, providing a more practical approach for point-of-care testing (POCT) in environmental monitoring.

In recent years, various strategies using smartphone-assisted colorimetric sensors have been developed for rapid, on-site detection of Ag(I) ion, showing promising application

Shanxi Provincial Key Laboratory of Chemical Biosensing, School of Chemistry and Chemical Engineering, Shanxi Datong University, Datong 037009, China. E-mail: lihuazhang888@163.com; feng-feng64@263.net

prospects. For example, Chen *et al.*[26] synthesized a smartphone-based NL-AuNCs colorimetric sensor using *N*-acetyl-L-cysteine (NAC) and DL-lipoic acid (LA) as precursors for detecting silver ions in environmental water samples. Xing *et al.*[27] integrated a deep learning algorithm into a smartphone-based sensing platform that uses nitrogen- and boron-*co*-doped carbon dots (N, B-CDs) prepared *via* a hydrothermal method from *o*-phenylenediamine and boric acid for quantitative visual analysis of silver ions. Jia *et al.*[28] developed a smartphone-assisted dual-mode sensor for monitoring Ag(I), based on orange-red-emitting carbon dots (or-CDs) prepared from *p*-aminobenzenesulfonic acid and *p*-phenylenediamine as precursors, achieving both fluorescence and colorimetric dual responses. Despite advances in sensitivity and selectivity, the practical deployment of these methods still faces significant challenges. The core issue lies in the complex and costly synthesis processes of gold nanoclusters (AuNCs) and carbon dots (CDs), manifested as: complicated synthetic procedures requiring multi-step reactions; reliance on specific precursors and ligands, such as *p*-phenylenediamine[29] and polyvinylpyrrolidone (PVP),[30] which are often expensive and suffer from poor water solubility or structural instability; high post-treatment demands, including dialysis or column chromatography for purification and surface functionalization to enhance recognition capability; and strong dependence on external detection systems,[31] with some carbon dots requiring UV excitation sources, increasing equipment dependency and operational barriers. These limitations hinder the widespread adoption of current sensors for point-of-care testing (POCT), especially in resource-limited or field-deployable monitoring scenarios. Thus, it is necessary to develop a smartphone-integrated, simple, purification-free, one-step synthetic colorimetric sensor for on-site real-time detection of Ag(I).

To overcome these limitations, we developed a smartphone-integrated point-of-care testing (POCT) system that enables rapid, highly selective, and sensitive detection of Ag(I) at room temperature using a "one-stone-three-birds" strategy for constructing functionalized AuNPs. Here, the selective use of ammonium thioglycolate (ATG) not only imparts a positive charge under pH 8.2, promoting electrostatic attraction to negatively charged AuNPs and accelerating initial aggregation through the ammonium group (NH_4^+), but also stabilizes the aggregates *via* a hydrogen-bonding network through its carboxyl group. Additionally, ATG serves as a high-affinity binding site for Ag(I), enabling specific target recognition and signal transduction through its thiol group. Specifically, ATG causes AuNPs to aggregate by forming strong covalent bonds, causing a color change from pink-red to gray-blue in the AuNPs solution. However, Ag(I) prefers binding with ATG over AuNPs, preventing this color change. This anti-aggregation mechanism enables detection of Ag(I) *via* a color change in the ATG-functionalized AuNP solution. The sensor's factors were optimized to improve sensitivity, and its analytical performance was evaluated and validated before testing on real samples. The proposed sensor offers new methods for simple and effective detection of Ag(I), with potential applications in environmental monitoring and biosensing.

2 Materials and methods

2.1 Chemicals and materials

Ammonium thioglycolate ($C_2H_7NO_2S$), gold chloride tetrachloride ($HAuCl_4 \cdot 4H_2O$), and trisodium citrate dihydrate ($C_6H_5Na_3O_7 \cdot 3H_2O$) were purchased from Aladdin Reagent Co., Ltd (Shanghai, China). Silver nitrate ($AgNO_3$) and other metal ions were purchased from Tianjin Guangfu Fine Chemical Institute (Tianjin, China). All the reagents were of AR grade unless otherwise specified. For all experiments, a phosphate-buffered saline (PBS) buffer solution containing Na_2HPO_4 and NaH_2PO_4 (0.01 M) was used, with the pH adjusted using NaOH solution (0.2 M).

2.2 Instruments

All images were captured using a HONOR X10 smartphone (HONOR Terminal Co., Ltd, Guangdong, China), which features a 48 MP camera with an *f*/1.8 aperture. The LED flash was positioned 15 cm from the sample during image capture. The JPEG file was then imported into an RGB color detection app (downloaded from the Play Store) on the same device, which provides RGB values (R = red, G = green, B = blue) to measure color intensity.

The UV-Visible absorbance spectra (UV-Vis) were recorded using a PerkinElmer Lambda 35 Spectrometer in the wavelength range of 200–800 nm. Next, transmission electron microscope (TEM) images were acquired using a JEM-1011 at an accelerating voltage of 120 kV. Additionally, pH measurements were performed with a PHS-3E pH meter (INESA Scientific Instrument Co., Ltd, Shanghai, China). The hydrodynamic size and zeta potential were measured using a Malvern Zetasizer Nano ZS90 (Malvern, United Kingdom). The control experiment for silver ion determination was performed using an AA-6800 atomic absorption spectrophotometer (AAS; Shimadzu Corporation, Tokyo, Japan). The optimal conditions for silver ion detection by AAS included a wavelength of 328.1 nm, a spectral bandwidth of 0.5 nm, a lamp current of 5.0 mA, a burner height of 7 mm, flame type: air-acetylene, an air compressor at 0.25 MPa, acetylene at 0.05 MPa, and an acetylene gas flow of 2200 mL min^{-1}.

2.3 Synthesis of AuNPs

Citrate-capped AuNPs (13 nm in diameter) were prepared using Frens' method.[32] Briefly, 10 mL of trisodium citrate (38.8 mM) was quickly added to 100 mL of boiling $HAuCl_4$ solution (1.0 mM) with vigorous stirring. Heating was stopped once the solution turned wine-red, and stirring was continued at 125 °C for 30 minutes. The solution was allowed to cool to room temperature while stirring, then filtered through a 0.22-μm membrane. The AuNPs were stored at 4 °C until use, and their concentration was measured as described previously.[33]

2.4 Preparation of the AuNPs modified with ATG

To functionalize AuNPs with ATG, 90 μL of AuNPs solution was mixed with 10 μL of ATG (2 μM) and 190 μL of PBS buffer (pH

8.2). The self-assembly reaction was conducted at room temperature with stirring at 400 rpm using a temperature-controlled shaker (MS-100) for 5 minutes to produce the AuNPs-ATG system. After incubation, the reaction mixture was analyzed immediately by UV-Vis spectroscopy to measure the absorbance ratio (A_{680}/A_{520}), which serves as a quantitative indicator of AuNP aggregation or surface modification.

2.5 Procedure for detection of Ag(I) using smartphone-assisted colorimetric sensor

An Ag(I) solution was prepared by dissolving silver nitrate in ultrapure water. A 10 μL aliquot of the Ag(I) solution at a predetermined concentration was added to 290 μL of citrate-stabilized AuNPs-ATG. The mixture was then shaken on an orbital shaker at 400 rpm for 5 minutes. After incubation, the color of the reaction mixture was recorded with a smartphone and analyzed using an RGB color detector to assess color intensity. After optimizing and evaluating the relationship between the R, G, and B values and Ag(I) concentration, the red-to-blue channel ratio (R/B) was selected as the key parameter for quantitative detection of Ag(I). Each experimental group was tested three times in parallel to minimize errors.

2.6 Ag(I) detection of real samples using smartphone-assisted colorimetric sensor

To assess the detection performance of the sensing strategy in real environmental samples, tap water and lake water were collected from our laboratory and Wenying Lake in Datong City, Shanxi Province, respectively. All real samples were pretreated by boiling and then centrifuged at 12 000 rpm for 10 minutes. Next, the samples were filtered through a 0.22-μm membrane to remove insoluble particles, producing a supernatant free of physical impurities. The AuNPs-ATG solution was then mixed with the pretreated real water samples containing the three target analytes. After a 5-minutes reaction, the color changes were visually recorded with a smartphone and analyzed using an RGB color detector to measure color intensity.

3 Results and discussion

3.1 Principle of smartphone-integrated quantitative detection platform for Ag(I) sensing

We have developed an integrated quantitative detection platform that utilizes smartphone image capture and a built-in RGB color analysis app. This method effectively detects Ag(I) ions with high sensitivity, employing a one-stone-three-birds strategy. Initially, AuNPs were synthesized through the classic citrate reduction of $HAuCl_4$. The citrate-stabilized AuNPs readily undergo ligand exchange with molecules containing functional groups such as heterocyclic oxygen (–O) and thiol (–SH).[34] Additionally, ATG, a small organic molecule featuring a sulfhydryl (–SH) group, a carboxyl ($–COO^-$) group, and ammonium ions (NH_4^+), was used as an innovative trifunctional reagent. It combines the roles of an aggregation inducer, recognition unit, and charge modulator. As shown in Scheme 1, the sensing mechanism depends on the competitive interaction between

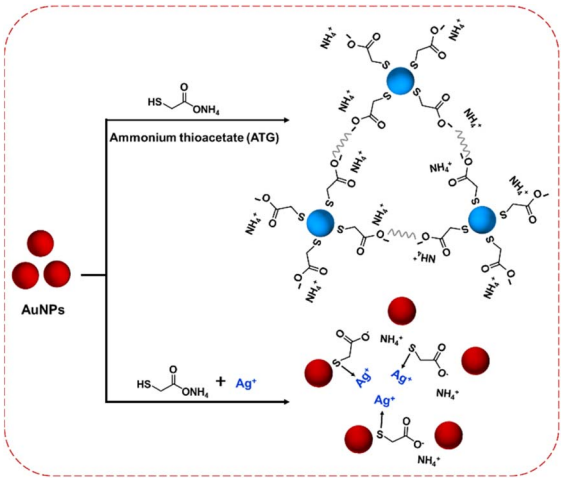

Scheme 1 Schematic illustration of a potential colorimetric sensing mechanism for Ag(I). Note: minor interfacial deprotonation may occur; charge compensation is automatically maintained *via* internal acid–base equilibrium.

ATG and AuNPs *versus* ATG and Ag(I) ions, which controls the aggregation or anti-aggregation behavior of the AuNPs. Specifically, when ATG is added to the AuNP solution, the –SH group forms Au–S bonds with the AuNP surface through coordination interaction.[35] Furthermore, electrostatic attraction causes ammonium ions to bind to negatively charged gold nanoparticles, accelerating the aggregation process. Hydrogen-bonding networks between the carboxyl oxygen atoms of neighboring ATG molecules can form intermolecular bridges, further promoting AuNP aggregation. The combined effects cause AuNPs to aggregate, shifting their surface plasmon resonance (SPR) peak to longer wavelengths and changing the solution color from pink to gray-blue. When Ag(I) ions are introduced, a color change from gray-blue to pink-red occurs, indicating that the aggregation of AuNPs is specifically inhibited. This is likely because the covalent interaction between the –SH groups of ATG and Ag(I) ions is stronger than that with AuNPs. According to the hard–soft acid–base (HSAB) theory, Ag(I) is a typical "soft acid", while the thiol group (–SH) in ATG acts as a "soft base". The soft–soft interaction between them is significantly stronger than the binding energy of the Au–S covalent bond.[36,37] Thermodynamic calculations show that the binding constant between Ag(I) and the thiol group is much higher than that between AuNPs and the thiol group.[38] Therefore, Ag(I) preferentially binds to the thiol group of ATG, forming a stable Ag–S coordination structure, which blocks the interaction between ATG and AuNPs, inhibits nanoparticle aggregation, and restores the pink color characteristic of dispersed AuNPs.

As shown in Fig. 1, the ATG-induced aggregation behavior of AuNPs was investigated through TEM imaging, DLS, and UV-vis spectroscopy. First, ATG contains multiple functional groups (NH_4^+, –COOH, and –SH) that can interact with the surface of AuNPs through electrostatic interactions, hydrogen bonding, and coordinate covalent bonding. As a result, ATG assembles on the AuNP surface *via* Au–S bonds, forming a dense "shell"

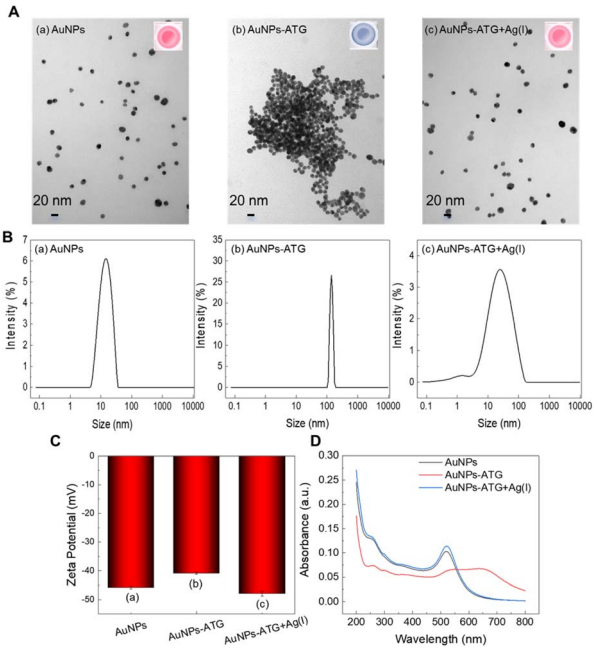

Fig. 1 (A) TEM micrograph, (B) DLS particle size distribution, (C) zeta potential, (D) UV-Vis absorbance spectrum of different reaction systems: AuNPs, AuNPs-ATG, and AuNPs-ATG + Ag(I); inset: photographs showing the sample color changes.

structure and partial neutralization of citrate-derived negative charges, which causes the zeta potential to increase from −45.8 mV (Fig. 1C(a)) to −40.8 mV (Fig. 1C(b)). The aggregation of AuNPs occurs rapidly due to assembly with ATG (Fig. 1A(b)), with particle size growing from 15 nm (Fig. 1B(a)) to 140 nm (Fig. 1B(b)), leading to a color change from pink-red (Fig. 1A(a)) to gray-blue (Fig. 1A(b)). At the same time, the AuNPs-ATG complex displays a clear shift in its surface plasmon resonance band and the peak characteristic of the blue solution appears at 680 nm, as shown in Fig. 1D (red line). Second, upon adding Ag(I), the strong coordination between Ag(I) and the thiol groups of ATG causes partial displacement or conformational change of ATG, restoring and even enhancing the negative surface charge, with the zeta potential decreasing further to −47.9 mV (Fig. 1C(c)). This leads to the re-dispersion of the AuNPs-ATG complex, recovery of the 520 nm peak, and reduction of the 680 nm peak (Fig. 1D, blue line), with the solution returning to pink-red (Fig. 1A(c)), allowing visual detection. These results demonstrate that ATG, with its unique properties, not only forms an assembling "shell" on the AuNP surface but also causes reversible aggregation and dispersion of AuNPs in the presence of Ag(I).

3.2 Experimental condition optimization

The colorimetric response of the smartphone-integrated platform was enhanced through systematic optimization of key experimental parameters, thereby improving the system's sensitivity. Each data point for the experimental parameters, pH, the concentration of ammonium thioglycolate, and the reaction time, was obtained by conducting experiments both with and without Ag(I) ions.

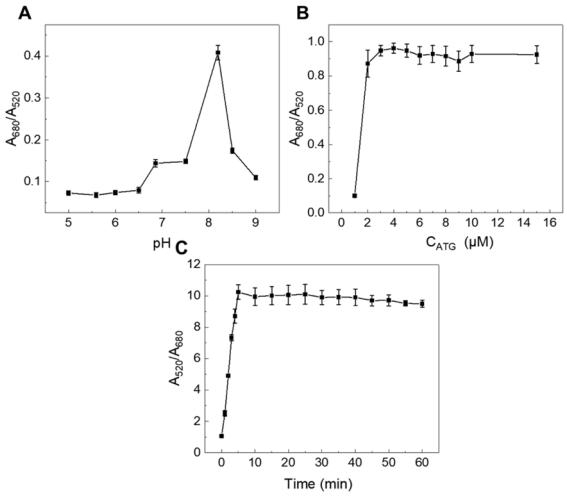

Fig. 2 (A) pH dependence (5.0–9.0) of the AuNPs-ATG sensor's response to Ag(I); (B) ATG concentration effect (1–16 μM) on AuNPs responsiveness; (C) reaction time influence on the Ag(I)-sensing performance of AuNPs-ATG.

As previously mentioned, the medium pH significantly affected interactions between ATG and Ag(I) and between AuNPs and ATG. The pH-dependent behavior of the AuNPs-ATG probe was studied over a pH range of 5.0 to 9.0. As shown in Fig. 2A, the reaction mixture contained 90 μL of AuNPs, 10 μL of ATG (2 μM), and 190 μL of PBS buffer (0. 01 M, pH 5.0–9.0). When citrate-stabilized AuNPs were used alone, with no signs of aggregation or color change, this confirmed that ATG mediates pH dependence (Fig. S1A). In addition, different pH-dependent effects on ATG-modified gold nanoparticles were observed, demonstrating pH-dependent aggregation and a red-shifted peak at 680 nm in the UV-Vis spectra (Fig. S1B). After 10 minutes, 10 μL of Ag(I) (10 μM) solution was added, the A_{680}/A_{520} absorbance ratio increased as pH rose from 5.0 to 8.2, and the partial solution's color changed from gray-blue to pink-red (Fig. S1C). Beyond pH 8.2 up to 9.0, the ratio decreased with increasing pH, the color shifted back from gray-blue to pink-red, the aggregation peak at 680 nm disappeared, and the surface plasmon resonance peak around 520 nm was restored, indicating that the gold nanoparticles re-dispersed and the aggregation was reversible. This shows that the colloidal stability of the AuNPs-ATG system responds to pH changes, demonstrating excellent pH-dependent behavior. Therefore, the optimal conditions were set at pH 8.2 with a PBS buffer concentration of 0. 01 M.

Furthermore, the modifier concentration is a crucial parameter in colorimetric chemosensors and must be optimized. The ideal ATG concentration should ensure complete surface saturation of AuNPs without leaving any free ATG in solution. In this study, a mixture of 90 μL of AuNPs and 200 μL of PBS (0.01 M, pH 8.2) buffer was combined with varying amounts of ATG to determine the optimal concentration. Fig. 2B shows that higher ATG concentrations cause a significant decrease in AuNPs absorption at 520 nm and the emergence of a new 680 nm absorption band caused by interparticle-

coupled plasmon effects in aggregated AuNPs due to free ATG molecules. At concentrations up to 2 μM, the 520 nm absorption of AuNPs-ATG remained mostly unchanged, indicating complete surface coverage by ATG molecules. This likely results from saturation of the AuNP surface –SH groups. Therefore, 2 μM was chosen as the optimal ATG concentration for further experiments.

Finally, response time is a key performance indicator for evaluating colorimetric sensing devices. The reaction kinetics of AuNPs-ATG with Ag(I) were studied by monitoring the color change over time. When Ag(I) was injected into the AuNPs-ATG solution, a rapid color change occurred. As shown in Fig. 2C, the absorbance ratio (A_{680}/A_{520}) steadily increased during the first 5 minutes of incubation with 10 μM Ag(I). No significant changes were observed with longer reaction times, indicating that a 5-minutes incubation is sufficient for Ag(I) detection. This is supported by UV-Vis spectral analysis, which revealed that Ag(I)-induced aggregation of AuNPs-ATG was complete within 5 minutes and remained stable thereafter. Therefore, a standard response time of 5 minutes was used for all subsequent Ag(I) detection tests.

3.3 Selectivity of the Ag(I) detection system

To enable reliable detection of Ag(I) in complex environmental water samples, a highly selective measurement method is crucial. For this, 290 μL of AuNPs-ATG solution was mixed with 10 μL of Ag(I) (10 μM) or other metal ion (10 μM), followed by incubating for 5 minutes. The interfering ions tested included Ag(I), Hg(II), Cu(II), Pb(II), Ca(II), Fe(II), Fe(III), Zn(II), Mg(II), Cd(II), Ni(II), Mn(II), Cr(III), Al(III), Cu(I), and Pd(II). As shown in Fig. 3, the addition of Ag(I) resulted in a noticeable color change of the colloidal solution from gray-blue to pink-red, whereas no significant color change was observed upon addition of the other metal ions, consistent with the AuNPs-ATG blank. The color changes were recorded using a smartphone, and the average color intensity of AuNPs was measured using an RGB color analyzer. The color intensity variations in the presence of different metal ions are presented as bar charts, clearly illustrating the sensor's selective response to Ag(I). The high selectivity can be explained at the molecular level by the soft–soft interaction between Ag(I) and –SH groups, consistent with the HSAB theory. Furthermore, this thermodynamic preference explains the high selectivity of the sensor. Although ions like Cu(I) and Pd(II) can also bind to –SH groups, their binding constants are significantly lower than those of Ag(I), preventing effective competition.

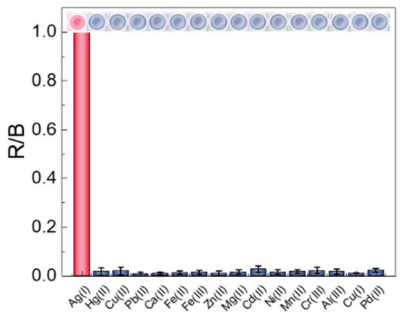

Fig. 3 Selectivity evaluation of the sensing system. The R/B ratio of the AuNPs-ATG system with a variety of metal ions (10 μM each); inset: photographs depicting the corresponding color changes.

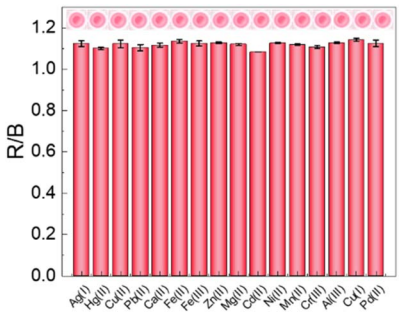

Fig. 4 Anti-interference evaluation of the sensing system. The R/B ratio of the AuNPs-ATG system for Ag(I) with potential interfering ions; inset: photographs showing the corresponding color changes.

3.4 Interference study of the Ag(I) detection system

To assess the anti-interference performance of the smartphone-integrated AuNPs-ATG platform for detecting Ag(I), we systematically evaluated its response to potential interfering metal ions (Hg(II), Cu(II), Pb(II), Ca(II), Fe(II), Fe(III), Zn(II), Mg(II), Cd(II), Ni(II), Mn(II), Cr(III), Al(III), Cu(I), and Pd(II)) under optimized conditions using a smartphone and a color detection app. Fig. 4 shows the R/B value and color change of the AuNPs-ATG sensor upon addition of Ag(I). The results clearly show nanoparticle re-aggregation and no significant color change in the presence of other metal ions, indicating that Ag(I) binds more strongly to ATG than other analytes. Therefore, the platform provides a reliable and effective method for quantitative detection of Ag(I) in real samples.

3.5 Sensitive detection of Ag(I) using a smartphone-integrated quantitative detection platform

To evaluate the sensitivity of the smartphone-integrated platform for quantitative detection of Ag(I), AuNPs-ATG were combined with solutions at various concentrations under optimized conditions. As shown in Fig. 5 (inset), different concentrations of Ag(I) were added to the AuNPs-ATG system, and color images were captured using a smartphone. These images were then cropped and recorded using a custom-developed app that outputs R, G, and B values. Subsequently, the relationship between the R/B value and Ag(I) concentration was calculated and fitted by the app. Fig. 5 shows that the R/B value has a linear relationship with Ag(I) in the range of 0–8 μM, with the equation $y = 0.0182x + 0.9675$ ($R^2 = 0.9947$). The limit of detection (LOD) was determined by spiking the lowest Ag(I) concentration into the solution until the signal response changed by 3 standard deviations (3σ). The resulting LOD was 10.4 nM. However, the LOD achieved with the smartphone-assisted method exceeds the tolerance limit (0.1 μM)

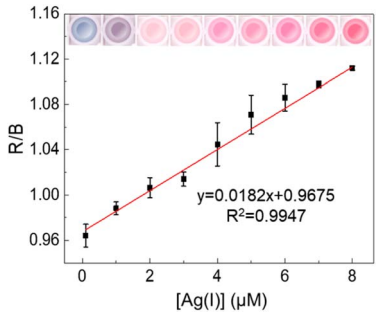

Fig. 5 The calibration curve showing the relationship between the R/B ratio and Ag(I) concentration (0–8 μM); inset: photographs illustrating the corresponding color changes.

recommended by the World Health Organization (WHO) for Ag(I) concentrations.

A comparison of the analytical performance of our colorimetric system with previously reported electrochemical, fluorescent, and smartphone-integrated methods for quantitative detection of Ag(I) is shown in Table 1. Notably, the proposed AuNPs-ATG platform operates under an "ultra-simple (smartphone + one-stone-three-birds)" strategy, featuring minimal operational complexity and extremely low equipment requirements. This stands in sharp contrast to conventional approaches that rely on "electrochemical workstations," "fluorescence spectrometers," or "complex synthesis procedures." By maintaining high analytical performance (strong specificity and high response efficiency) and the design significantly enhances detection convenience and on-site applicability, thereby highlighting the innovative advantage of achieving rapid, field-deployable analysis without compromising sensing performance.[39]

3.6 Application of the assay in environmental monitoring

The smartphone-integrated detection method developed for analyzing Ag(I) was tested on real environmental samples. Tap water (Shanxi Provincial Key Laboratory of Chemical Biosensing, Shanxi, China) and lake water (Wenying Lake Reservoir, Datong City, Shanxi Province) were analyzed using this method. The samples were initially filtered through a 0.22-μm membrane and subjected to 20-minutes boiling for chlorine gas removal. Subsequently, varying concentrations of Ag(I) solutions were introduced into all prepared samples. Under optimal conditions, this method was employed to determine the concentration of Ag(I). The signal intensity of the AuNPs solution was measured using a smartphone RGB color-detection app after the sample was added. The amount of Ag(I) in the different water samples was determined using a standard calibration curve, as shown in Table 2. To verify the method's accuracy, a control experiment was also conducted using atomic absorption spectroscopy (AAS). The linear detection range for Ag(I) by AAS was from 1×10^{-7} mol L^{-1} to 9×10^{-6} mol L^{-1}, with a calibration curve equation of $\Delta A = 0.0180$ C–0.0186 (C: μM), $R^2 = 0.9983$, and a detection limit of 0.05 μM. The AAS data are also presented in Table 2. At a 95% confidence level, the *t*-test results show no significant difference between this approach and AAS. Recovery percentages ranged from 96.21% to 97.16% for tap water samples and from 98.79% to 103.48% for lake water samples. Overall, the smartphone-based detection assay produced results consistent with the AAS method.

Table 1 Comparison of AuNPs-based assays for detecting Ag(I)

Methods	Target	Linear range	Detection limit	Method complexity/equipment requirements	Ref.
Electrochemistry	Ag(I)	0.25–2 μM	106 nM	Complexity/electrochemical workstation	16
Electrochemistry	Ag(I)	0–300 μM	0.21 nM	Complexity/electrochemical workstation	17
Electrochemistry	Ag(I)	100 fM–1 μM	35×10^{-6} nM	Complexity/electrochemical workstation	18
Fluorescence	Ag(I)	0–3 nM	0.25 nM	Complexity/fluorometer	22
Fluorescence	Ag(I)	1–100 nM	0.8 nM	Complexity/fluorometer	23
Fluorescence	Ag(I)	0.3–100 nM	0.08 nM	Complexity/fluorometer	24
Fluorescence	Ag(I)	0.125–12.5 μM	40 nM	Complexity/fluorometer	25
Smartphone-assisted colorimetry	Ag(I)	0.002–200 μM	1.3 nM	Complexity/smartphone	26
Smartphone-assisted colorimetry	Ag(I)	0.039–70 μM	39 nM	Complexity/smartphone	27
Smartphone-assisted colorimetry	Ag(I)	10–80 μM	780 nM	Complexity/smartphone	28
Smartphone-assisted colorimetry	Ag(I)	0–8 μM	10.4 nM	Simplicity + "one-stone-three-birds"/smartphone	This work

Table 2 Determination of Ag(I) in tap and lake water

			Tap water				Lake water			
	Samples	Added (μM)	Measured (μM)	Recovery (%)	RSD (%)	AAS (μM)	Measured (μM)	Recovery (%)	RSD (%)	AAS (μM)
Ag(I)	1	2.00	1.99	96.37	0.68	1.97	2.14	103.48	0.79	1.99
	2	3.00	2.95	96.21	0.69	2.99	3.03	98.79	1.41	3.04
	3	4.00	3.96	97.16	0.29	3.90	4.16	102.44	0.55	3.95

Therefore, this method is well-suited to detecting Ag(I) ions in real water samples.

4 Conclusions

In conclusion, a smartphone-integrated point-of-care testing (POCT) system was developed for the rapid, highly selective, and sensitive detection of Ag(I) ions at room temperature, using a "one-stone-three-birds" strategy with ATG as a multifunctional ligand to assemble and functionalize gold nanoparticles (AuNPs). This method removes the need for bulky spectrometric instruments and complicated synthetic procedures. Transmission electron microscopy (TEM) confirmed the successful synthesis and modification of AuNPs and AuNPs-ATG, confirming the structural integrity of the sensing platform. Interestingly, Ag(I) detection was indicated by a more noticeable color change from gray-blue to red in the AuNPs probes, using only commercially available materials and common equipment. The results showed that the AuNPs-ATG sensor had high sensitivity, with a detection limit of 10.4 nM for Ag(I), well below the WHO standard of 0.93 μM. This low-cost, instrument-free approach marks a major advancement in on-site environmental monitoring by overcoming key challenges. Notably, this approach can be extended to detect other metal ions using the HSAB (Hard and Soft Acid–Base) theory, which our team is currently investigating. This work not only introduces a new method for Ag(I) detection but also demonstrates that strategies such as multifunctional ligand selection and smartphone integration can serve as models for developing rapid, on-site sensors for various environmental pollutants.

Author contributions

Lihua Zhang: conceptualization, methodology, writing – original draft, funding acquisition. Jiang Li: conceptualization, review & editing. Tengyan Gao: investigation, methodology, datacuration. Liu Wei: validation. Zirui Zhang: validation. Zezhong Chen: review & editing. Feng Feng: review & editing, funding acquisition. All authors approved the final version of the manuscript.

Conflicts of interest

The authors declare no competing financial interest.

Data availability

The authors confirm that the data supporting the findings of this study are available within the article and/or its supplementary information (SI). Supplementary information: the effect of pH. See DOI: https://doi.org/10.1039/d6ra02021f.

Acknowledgements

This study was funded by the National Natural Science Foundation of China (22476118), the Innovation and Entrepreneurship Training Program for College Students in Shanxi Province (XDC2023121), and the Fundamental Research Program of Datong City (2023058).

Notes and references

1 M. Rievaj, E. Culková, D. Šandorová, J. Durdiak, R. Bellová and P. Tomčík, *Nanomaterials*, 2023, **13**, 1262.
2 Z. Pan, T. Gong and P. Liang, *Circ. Res.*, 2024, **134**, 1160–1178.
3 R. AbhijnaKrishna and S. Velmathi, *Coord. Chem. Rev.*, 2022, **459**, 214401.
4 S. Chen, R. Xie, M. Tian, R. Yan, Z. Wang, R. Xie and F. chai, *Spectrochim. Acta, Part A*, 2025, **332**, 125862.
5 E. N. Benton, S. B. Marpu and M. A. Omary, *ACSAppl. Mater. Interfaces*, 2019, **11**, 15038–15043.
6 N. Agrawal, N. Soleja, R. Bano, R. Nazir and M. Mohsin, *ACS Omega*, 2021, **6**, 14164–14173.
7 M. B. Tayemeh, M. Esmailbeigi, I. Shirdel, H. S. Joo, S. A. Johari, A. Banan, H. Nourani, H. Mashhadi, M. J. Jami and M. Tabarrok, *Chemosphere*, 2020, **238**, 124576.
8 E. Tan, P. Yin, X. Lang, X. Wang, T. You and L. Guo, *Analyst*, 2012, **137**, 3925–3928.
9 Q. H. Ying, H. M. Lan, T. Xue, H. L. Jiao and C. Xia, *Anal. Sci.*, 2013, **29**(10), 991–996.
10 P. Zheng, M. Li, R. Jurevic, S. K. Cushing, Y. Liu and N. Wu, *Nanoscale*, 2015, **7**(25), 11005–11012.
11 C. Wu, C. Xiong, L. Wang, C. Lan and L. Ling, *Analyst*, 2010, **135**(10), 2682–2687.
12 C. C. Chang, S. Lin, S. C. Wei, C. S. Yu and C. W. Lin, *Anal. Bioanal. Chem.*, 2012, **402**(9), 2827–2835.
13 K. Nakata, B. Hashimoto, H. Uchihara, Y. Okamoto, S. Ishizaka and T. Fujiwara, *Talanta*, 2015, **138**, 279–284.
14 X. Men, C. X. Wu, X. Zhang, X. Wei, M. L. Chen, T. Yang and J. H. Wang, *Anal. Chim. Acta*, 2021, 338540.
15 K. Ramos, L. Ramos and M. M. Gomez-Gomez, *Food Chem.*, 2017, **221**, 822–828.
16 L. A Wasiewska, I. Seymour, B. Patella, R. Inguamta and A. O'iordan, *Sens. Actuators, B*, 2021, **333**(1), 129531.
17 J. Wang, H. Li, W. Liao, K. Liu, H. Li, R. A. Geioushy, R. Tahawy, M. Sayed, L. Jiang and J. Fu, *Sens. Actuators, B*, 2024, **399**, 134796.
18 X. Niu, M. Li, T. Liu, Y. Yang, J. Lu and X. Zhang, *Sens. Actuators, B*, 2025, **426**, 137019.
19 J. Y. Li, Y. J. Wang, L. Cai, Z. Y. Lin, Z. X. Jiang, P. M. Liu, W. R. Cai, D. T. Wu, Z. Z. Yin and Y. Kong, *J. Environ. Chem. Eng.*, 2025, **13**(6), 120005.
20 M. Mohammadpour and H. Razmi, *J. Porous Mater.*, 2022, **29**(5), 1575–1587.
21 D. Yang, T. Zhou, Y. Tu and J. Yan, *Microchim. Acta*, 2021, **188**, 212.
22 R. Pavadai, A. Amalraj, S. Subramanian and P. Perumal, *ACS Appl. Mater. Interfaces*, 2021, **13**, 31710–31724.
23 Z. Tao, G. Yi, C. Zeng, Q. Zhuang and Y. Wang, *Sens. Actuators, B*, 2022, **369**, 132382.
24 Y. Zhang, K. Zhou, Y. Qiu, L. Xia, Z. Xia, K. Zhang and Q. Fu, *Sens. Actuators, B*, 2021, **339**, 132382.

25 T. Liu, L. Fu, C. Y, M. Wu, L. Chen and N. Niu, *Devoted to the Application of Microtechniques in All Branches of Science*, 2022, p. 174.
26 S. Chen, R. Xie, M. Tian, R. Yan, Z. Wang, R. Xie and F. Chai, *Spectrochim. Acta, Part A*, 2025, **332**, 125862.
27 H. Xing, Y. Zhang, Y. Wang, S. Gao, X. Liu, H. Hu, J. Chen, H. He and D. Chen, *Microchem. J.*, 2025, **209**, 112782.
28 J. Jia, H. Wang and R. Quan, *Mater. Today Chem.*, 2023, **33**, 101730.
29 W. Ni, G. X. Li, Y. T. Zhao, Y. Fang, S. Huang, F. X. Wei and Q. Xiao, *Colloids Surf., A*, 2025, **727**, 138422.
30 C. Wu, S. Zhang, M. Liu and J. He, *Carbon*, 2024, **230**, 9.
31 S. Zhang, J. Li, J. Zhou, P. Xu, Y. Li, Y. Zhang and S. Wu, *Talanta*, 2025, **282**, 126983.
32 G. Frens, *Controlled Nucleation for the Regulation of the Particle Size in Monodisperse Gold Suspensions*, Macmillan Company, 1973, vol. 241, pp. 20–22.
33 J. Shang and X. Gao, *Chem. Soc. Rev.*, 2014, **43**, 7267–7278.
34 Y. Li, P. Wu, X. Hu, Z. P. Zhang and X. H. Zhong, *Talanta*, 2011, **84**(2), 508–512.
35 K. Uvdal, P. Bod and B. Liedberg, *J. Colloid Interface Sci.*, 1922, **149**(1), 162–173.
36 H. Mahmoudi, M. Bahram and R. Dadashi, *Inorg. Chem. Commun.*, 2024, **167**, 112834.
37 C. Battocchio, C. Meneghini, I. Fratoddi, I. Venditti, M. V. Russo, G. Aquilanti, C. Maurizio, F. Bondino, R. Matassa and M. Rossi, *J. Phys. Chem. C*, 2012, **116**, 19571–19578.
38 S. Wang, X. Wang, Z. Zhang and L. Chen, *Colloids Surf., A*, 2015, **468**, 333.
39 N. Peamaroon, J. Jakmunee and N. Moonrungsee, *J. Anal. Test.*, 2021, **5**, 379–386.